Papers

Power and Modulation Bandwidth of GaAs–AlGaAs High-Radiance LED's for Optical Communication Systems

TIEN PEI LEE, SENIOR MEMBER, IEEE, AND ANDREW G. DENTAI, MEMBER, IEEE

Abstract—**We present an analytical model for GaAs–AlGaAs double heterostructure high-radiance LED's intended for use in optical communication systems. This model takes all the important device and material parameters, such as self absorption, heterointerfacial recombination, doping concentration, active-layer width, injection carrier density, and carrier confinement into account. A theoretical discussion of the effect of these parameters on LED output power and modulation bandwidth is given along with experimental results which are in good agreement with the model. The best high-output 50-μm LED's (biased near saturation) emitted 15 mW into the air with a radiance of 200 W/cm^2 · sr (highest ever reported for a surface emitter LED) and a modulation bandwidth of 17 MHz; the highest bandwidth obtained was 170 MHz at 2-mW output.**

I. Introduction

SINCE the first report of GaAs–AlGaAs high-radiance LED's by Burrus and Miller [1] in 1971, these devices have received increasing attention as possible sources for use in lightwave communication systems. The most important characteristics of such small-area devices to be considered for this application are output power (or efficiency) and modulation bandwidth. In this paper we discuss some of the device parameters relevant to LED performance, with particular attention paid to those important in communication sources. These parameters include self absorption, heterointerfacial recombination, doping concentration, active-layer thickness, injection carrier density, and carrier confinement. Certain aspects of these parameters have been discussed in a number of publications recently: Harth and Heinen [2] have studied the effect of absorption and surface recombination in single heterostructure LED's, and the frequency response of these devices [3]; King, SpringThorpe, and Szentesi [4] have presented experimental results of efficiency and risetime of double heterostructure (DH) LED's as a function of hole concentration in the active region, but no analysis was given; Ettenberg and Kressel [5] have considered the interfacial recombination of AlGaAs-GaAs heterojunctions; minority carrier diffusion length as a function of carrier concentration was measured by Ettenberg, Kressel, and Gilbert [6], by Casey, Miller, and Pinkas [7] and by Zucker, Laner, and Schlafer [8]; parasitic effects of the frequency response of Burrus-type LED's were analyzed and reported by Lee [9], and by Burrus, Lee, and Holden [10]; high-power performances of LED's was reported by King *et al.* [4], whereas high-frequency performances were reported by Goodfellow and Mabbitt [11] and by Lockwood, Wittke, and Ettenberg [12].

First, we present a basic model describing internal efficiency and carrier lifetime in relation to self absorption and interfacial recombination. The criterion for achievement of high efficiency is that the interfacial recombination velocity at the heterostructure interfaces be less than 10^4 cm/s. The self-absorption becomes important when the interfacial recombination rate is small and the doping in the active region is low.

Second, we discuss the modulation bandwidth of LED's. If the question of the parasitic effects can be set aside, the fundamental upper limit on bandwidth is set by the rate of recombination. The desired wide bandwidth can be obtained by increasing the nonradiative recombination rate, and this may be done, for example, by increasing the interfacial recombination rate [2] or by introducing Auger recombinations [11] (through excessive doping). In either case, the bandwidth is increased at the expense of efficiency and power. On the other hand, the bandwidth also can be increased by increasing the radiative recombination rate through heavy injection (bimolecular recombination) [5], which results in both higher efficiency and wide bandwidth. Obviously the latter is a better approach, but it can be achieved only when the active region is lightly doped.

Third, we consider the heterostructure barrier height necessary to confine injected carriers in the active region at high temperatures. The active layer thickness as well as the doping concentrations in the ternary layers are considered. The model takes both diffusion and drift terms into account for the determination of the leakage current.

Finally, we present experimental results for devices designed on the basis of the foregoing discussions. These experimental results support the applicability of our model.

Manuscript received November 24, 1976; revised August 25, 1977 and February 7, 1977.

The authors are with Bell Laboratories, Crawford Hill Laboratory, Holmdel, NJ 07733.

0018-9197/78/0300-0150$00.75 © 1978 IEEE

II. Internal Quantum Efficiency and Effective Carrier Lifetime

It has been shown [13] that self absorption plays a major role in the design of some types of light emitting diodes. In direct bandgap materials such as GaAs the peak of the emission shifts toward the high-energy side of the band edge in heavily doped n-type material, while the peak of the emission shifts toward the low-energy side of the band edge in heavily doped p-type material [14]. In either case, the absorption coefficient α at the emission peak is in the range $10^3\ \text{cm}^{-1} < \alpha < 10^4\ \text{cm}^{-1}$ [15]. The light generation region usually extends to several diffusion lengths which, in the lightly doped ($\sim 10^{17}\ \text{cm}^{-3}$) p-type GaAs, is 6-8 μm [7]. Thus, self absorption becomes appreciable. One obvious reason for the higher external efficiency observed in double heterostructure LED's (relative to diffused homostructures) is the reduction of the self absorption due to an ability to produce thin active regions.

In our analysis, we assume a one-dimensional model which should be applicable to LED's having a large active-area-to-thickness ratio as exists in the Burrus-type device. This LED structure is depicted in Fig. 1(a), and Fig. 1(b) gives the detail of the relevant layers of a one-dimensional model. While the choice of a p-type active layer is important for homostructure diffused LED's (the emission-peak shift toward longer wavelength reduces the self absorption) it is rather arbitrary in a DH device. However, even in DH LED's a p-type active layer is preferable since in GaAs electron injection is more efficient than hole injection. As indicated in Fig. 1(b) the generated light can radiate through either the p- or n-passive window layer, but there is a slight advantage in taking the output from the n-passive layer because of its lower free-carrier absorption. Our calculations, however, are based on the absorption in the active layer only. Its effect on the efficiency for light extracted either from the p- or from the n-passive window layers are presented in the following analysis.

We have assumed that recombination in the space-charge region is negligible and that electron diffusion current dominates the junction current. The steady-state continuity equation is

$$D\frac{d^2n}{dx^2} - \frac{n}{\tau} = 0 \tag{1}$$

where n is the electron density in cm^{-3}, D is the electron diffusion constant in cm^2/s, and τ is the bulk recombination lifetime in seconds. The boundary conditions, assuming equal surface recombination velocity s in cm/s at both heterointerfaces, are

$$-\left.\frac{dn}{dx}\right|_{x=0} = \frac{J}{eD} - \frac{s}{D}n(0) \tag{2}$$

$$\left.\frac{dn}{dx}\right|_{x=w} = -\frac{s}{D}n(w) \tag{3}$$

where J is the injected current density at the p-n heterojunction and e is the electronic charge.

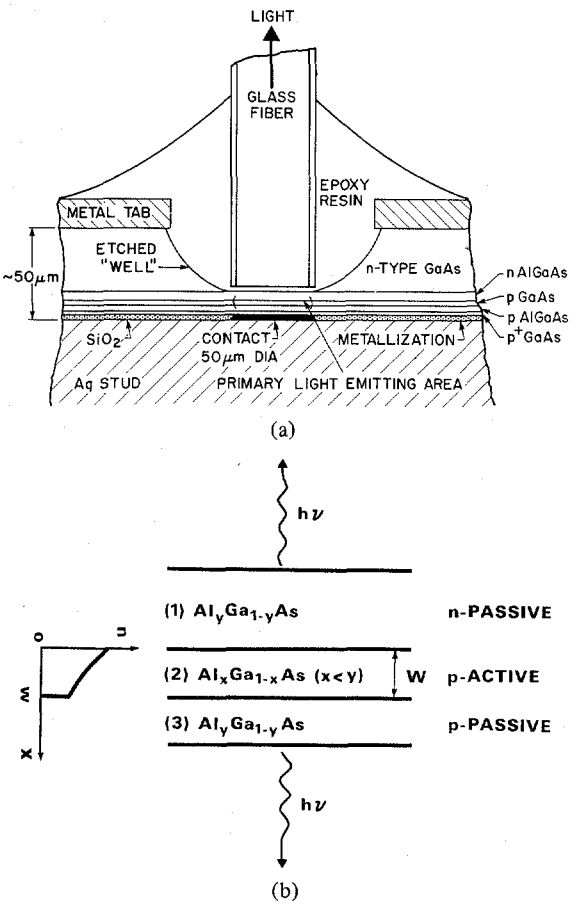

Fig. 1. (a) Construction of a GaAs–AlGaAs DH Burrus-type LED. (b) A one-dimensional model of the DH layers used in the analysis.

The electron density can be obtained readily from (1)-(3), and is given by

$$n(x) = \frac{JL}{eD}\left\{\frac{\cosh\left(\frac{w-x}{L}\right) + \frac{Ls}{D}\sinh\left(\frac{w-x}{L}\right)}{\left[\left(\frac{Ls}{D}\right)^2 + 1\right]\sinh\frac{w}{L} + \frac{2Ls}{D}\cosh\frac{w}{L}}\right\} \tag{4}$$

where L is the electron diffusion length ($L = \sqrt{D\tau}$) in centimeters. The average electron density in the active region is

$$\bar{n} = \frac{1}{w}\int_0^w n(x)\,dx = \frac{J}{e}\frac{\tau_{\text{eff}}}{w} \tag{5}$$

where τ_{eff}, given by

$$\tau_{\text{eff}} = \tau\left\{\frac{\sinh\frac{w}{L} + \frac{Ls}{D}\left(\cosh\frac{w}{L} - 1\right)}{\left[\left(\frac{Ls}{D}\right)^2 + 1\right]\sinh\frac{w}{L} + \frac{2Ls}{D}\cosh\frac{w}{L}}\right\} \tag{6}$$

is the average effective carrier lifetime when surface recombinations are important. When the surface recombination velocity is smaller than the diffusion rate, i.e., $Ls/D \ll 1$ [16], (6) can be reduced to a simple form, namely

$$\frac{1}{\tau_{\text{eff}}} = \frac{1}{\tau} + \frac{2s}{w}. \tag{7}$$

Equation (7) indicates the reduction in the carrier lifetime due to nonradiative, heterointerface recombination.

The peak light intensity of frequency ν at the p-n heterojunction, taking into account self absorption in the recombination region, can be written as

$$P = \frac{h\nu}{\tau_r} \int_0^w n(x)\, e^{-\alpha x}\, dx \tag{8}$$

where τ_r is the radiative recombination lifetime and α is the absorption coefficient at the emission-peak wavelength.

Using (4) for $n(x)$ in (8), we obtain

$$P = \left(\frac{h\nu}{e}\right) \eta_i J = \left(\frac{h\nu}{e}\right) \eta_0 \eta_{\mathrm{DH}}^n J \tag{9}$$

where $\eta_0 = \tau/\tau_r$ is the internal quantum efficiency when $s = 0$, and $\alpha = 0$. η_i is the reduced internal quantum efficiency when the interface recombinations and self absorption are significant, and $\eta_{\mathrm{DH}}^n = \eta_i/\eta_0$ is the internal quantum efficiency reduction factor. The subscript denotes DH and the superscript denotes the light extraction from the n-side passive layer.

$$\eta_{\mathrm{DH}}^n = \frac{1}{2\left[(S^2+1)\sinh\frac{w}{L} + 2S\cosh\frac{w}{L}\right]} \cdot \left\{\frac{1+S}{1+\alpha L}\left(1 - e^{-w(1+\alpha L)/L}\right) e^{w/L} - \frac{1-S}{1-\alpha L}\left(1 - e^{w(1-\alpha L)/L}\right) e^{-w/L}\right\} \tag{10}$$

where we have used $S = Ls/D$, the normalized form for the interface recombination velocity.

For single heterostructure (SH) devices, where the electron confinement is accomplished by a heterointerface at the p-p boundary while the electron injection occurs at a homostructure p-n junction, (10) becomes

$$\eta_{\mathrm{SH}}^n = \frac{1}{2\left(\sinh\frac{w}{L} + S\cosh\frac{w}{L}\right)} \cdot \left\{\frac{1+S}{1+\alpha L}\left(1 - e^{-w(1+\alpha L)/L}\right) e^{w/L} - \frac{1-S}{1-\alpha L}\left(1 - e^{w(1-\alpha L)/L}\right) e^{-w/L}\right\} \tag{11}$$

where the subscript denotes SH.

If the light is emitted from the p-p side of the active region, opposite the plane of electron injection, the reduction in internal quantum efficiency for DH structures becomes

$$\eta_{\mathrm{DH}}^p = \frac{1}{2\left[(S^2+1)\sinh\frac{w}{L} + 2S\cosh\frac{w}{L}\right]} \cdot \left\{\frac{1-S}{1+\alpha L}\left(1 - e^{-w(1+\alpha L)/L}\right) - \frac{1+S}{1-\alpha L}\left(1 - e^{w(1-\alpha L)/L}\right)\right\} \tag{12}$$

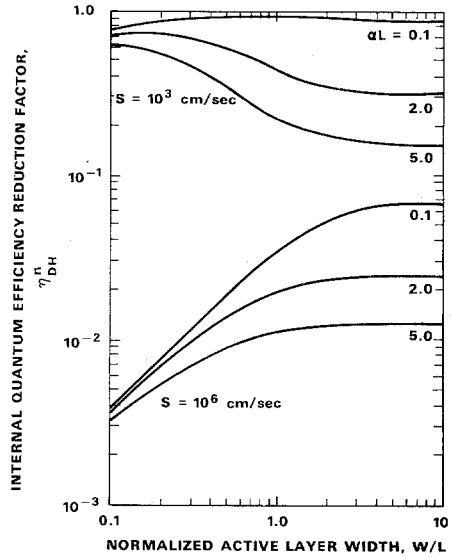

Fig. 2. Reduction factor of the internal quantum efficiency as a function of the normalized active layer width when the light is extracted from the side of the plane of injection in a DH LED. Parameters: s is the interfacial recombination velocity, α is the absorption coefficient, and L is the diffusion length of minority carriers.

where the superscript denotes the light extraction from the p-side passive layer. For SH structures, the internal quantum efficiency reduction factor reduces to the form given by [17]

$$\eta_{\mathrm{SH}}^p = \frac{1}{2\left[\sinh\frac{w}{L} + S\cosh\frac{w}{L}\right]} \cdot \left\{\frac{1-S}{1+\alpha L}\left(1 - e^{-w(1+\alpha L)/L}\right) - \frac{1+S}{1-\alpha L}\left(1 - e^{w(1-\alpha L)/L}\right)\right\}. \tag{13}$$

Figs. 2 and 3 are plots of η_{DH}^n versus w/L based on (10) for DH LED's. In these plots, we have assumed a value for D to be 80 cm^2/s in GaAs. The value of s ranges from 10^3 cm/s for a good heterointerface to 10^6 cm/s for a free surface (GaAs-air interface). Values of α and L are functions of doping concentration. These values are taken from [15] as follows: $\alpha \sim 10^3$ cm^{-1} and $L \sim 1 \times 10^{-4}$ cm for 10^{19} cm^{-3} p-type doping; $\alpha \sim 4 \times 10^3$ cm^{-1}, and $L \sim 5 \times 10^{-4}$ cm for 10^{18} cm^{-3} doping; and $\alpha \sim 7 \times 10^3$ cm^{-1}, $L = 7 \times 10^4$ cm for 10^{17} doping. Thus, the corresponding values of αL are 0.1, 2.0, and 5.0 shown on the curves in Figs. 2 and 3.

Fig. 4 is for light emission from the p-side of the active region, opposite to the plane of electron injection. The parameters used are the same as those in the previous figures. Comparing these figures, we can make the following remarks.

1) Surface recombination severely reduces both the efficiency and the total recombination lifetime, especially for devices with a very thin active region. For $s \geqslant 10^5$ cm/s, the interfacial recombination dominates. As a result, carrier confinement cannot be achieved by narrow heterostructures. Effective confinement can be achieved in narrow heterostructure only if $s \leqslant 10^4$ cm/s.

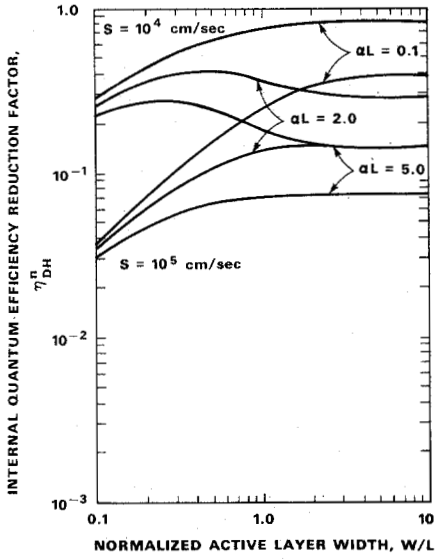

Fig. 3. Reduction factor of the internal quantum efficiency as a function of the normalized active layer width when the light is extracted from the side of the plane of injection in a DH LED. Parameters: s is the interfacial recombination velocity, α is the absorption coefficient, and L is the diffusion length of minority carriers.

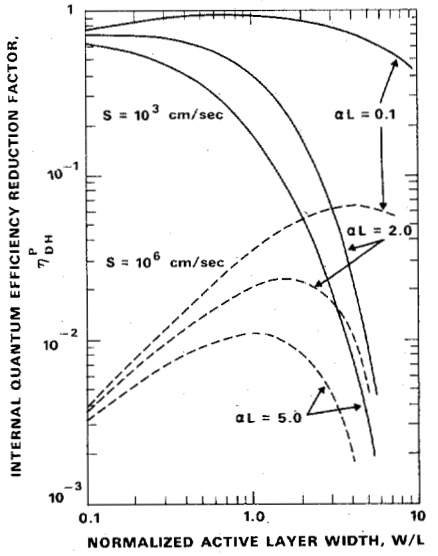

Fig. 4. Reduction factor of the internal quantum efficient as a function of the normalized active layer width when the light is extracted from the opposite side of the plane of injection in a DH LED. Parameters: s is the interfacial recombination velocity, α is the absorption coefficient, and L is the diffusion length of minority carriers.

2) For $s \leqslant 10^3$ cm/s self absorption becomes important particularly in lightly doped active regions. In this case the active region should be made thin ($\leqslant 1$ μm) compared to the electron diffusion length. However, for very thin active layers, the bandgap difference between the confining layers and the active layer must be large enough to prevent carrier leakage (further discussion in Section IV).

3) For $s = 10^4$ cm/s, an optimum active region thickness exists between 2 and 2.5 μm and is not much dependent on the doping concentrations. For $s \geqslant 10^5$ cm/s, the efficiency increases with active region thickness up to $w = 3L$, above which the efficiency levels off.

4) If the light is to be extracted from the p-side of the active region, the efficiency decreases at large w/L because of the increased absorption with large thickness. If $s \geqslant 10^4$ cm/s, the maximum efficiency occurs at $w \simeq L$. If $s \leqslant 10^3$ cm/s, the efficiency increases with decreasing thickness of the active region, and there is no appreciable difference in efficiency between the light extraction from the p-side and that from the n-side.

III. Modulation Bandwidth and Power Bandwidth Product

Intensity modulation of the light output can be accomplished by direct modulation of the injection current provided the rate of variation of the current is slower than the rate of recombination of the injected electrons and holes. Parasitic elements such as the space-charge capacitance causes a delay of the carrier injection into the junction, and consequently a delay in the light output [9]. This delay becomes negligible if a constant forward bias is maintained so that the modulation bandwidth of the LED is limited only by the carrier recombination time. If the current is modulated at an angular frequency ω, the intensity of the light output will vary with ω as [18], [19]

$$|I(\omega)| = \frac{I(0)}{\sqrt{1 + (\omega\tau_{\text{eff}})^2}} \tag{14}$$

where $I(0)$ is the light intensity at zero modulation frequency and τ_{eff} is the effective carrier lifetime. Equation (14) is valid when the diode is forward biased sufficiently to make the parasitic capacitance negligible. This occurs when the recombination time constant due to parasitic capacitance is smaller than the carrier recombination time, i.e., $(nKT/eI)\,C < \tau$ where the parasitic capacitance C is approximately 200 pF (9). At 5-mA forward current the RC time constant would be about 2 ns. The modulation bandwidth is defined as the frequency at which the detected electrical power ($\sim I^2(\omega)$) is half of that at zero modulation frequency, that is to say $I^2(\omega) = \frac{1}{2} I^2(0)$, thus the bandwidth Δf is

$$\Delta f = \frac{\Delta\omega}{2\pi} = \frac{1}{2\pi\tau_{\text{eff}}}. \tag{15}$$

If we assume that interface recombination is the dominating nonradiative recombination process, we can rewrite (7) as

$$\frac{1}{\tau_{\text{eff}}} = \frac{1}{\tau_r} + \frac{2s}{w} \tag{16}$$

where τ_r, the radiative recombination time, is inversely proportional to the sum of electron and hole concentrations at thermal equilibrium and the injected carriers in the recombination region [20]. τ_r can be written as [21]

$$\tau_r = \frac{[(n_0 + p_0)^2 + 4J/Bew]^{1/2} - (n_0 + p_0)}{2J/ew} \tag{17}$$

where $(n_0 + p_0)$ are electron and hole concentrations at thermal equilibrium, J is the injected current density, and B is the recombination probability. Thus, in the case of negligible nonradiative recombination, the bandwidth Δf is proportional to

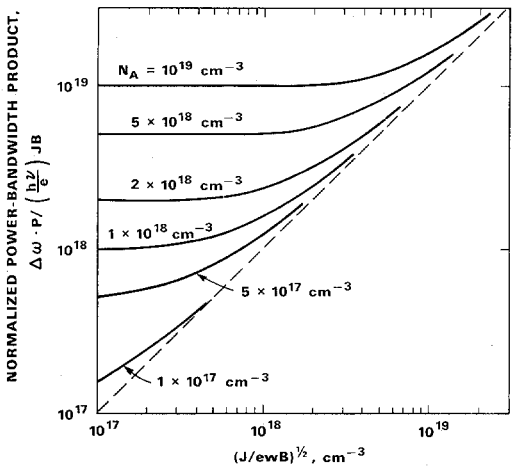

Fig. 5. Normalized power bandwidth product of an LED as a function of the injected electron density in the p-active region. The parameters are acceptor concentrations. The $(\Delta\omega \cdot P)$ product increases with electron injection.

the doping concentration at low injection levels and increases to $(JB/ew)^{1/2}/2\pi$ at high injection levels.

It is interesting to consider the power bandwidth product of LED's. Using (9) and multiplying both sides by $\Delta f = 1/2\pi\tau_r$, we obtain

$$\Delta f \cdot P = \left| \frac{h\nu}{2\pi e} \right| J \cdot \frac{1}{\tau_r} \tag{18}$$

when the interface recombination and self absorption are negligible ($\eta_{\mathrm{DH}}^n = \eta_0 = 1$). Using (17) for τ_r, (18) becomes

$$\Delta f \cdot P = \left| \frac{h\nu B}{2\pi e} \right| J(n_0 + p_0) \tag{19}$$

at low injection, and

$$\Delta f \cdot P = \left| \frac{h\nu B}{2\pi e} \right| J \left(\frac{J}{ewB} \right)^{1/2} \tag{20}$$

at high injection. When the interface recombination (or any other nonradiative recombination) is large, the bandwidth increases by a factor of η_{DH}^n, but the power is reduced by the same factor so that the net power bandwidth product remains unchanged. Comparing (19) and (20), we can conclude that the product $\Delta f \cdot P$ is proportional to (JN_A), at small currents and high doping concentrations where $N_A \approx (n_0 + p_0)$ is the acceptor doping concentration, and that $\Delta f \cdot P$ becomes proportional to $(J^{3/2}/w^{1/2})$ when the injected electron density is higher than the doping concentration. The power bandwidth product is improved by heavy injection as can be seen from Fig. 5 where the ordinate is $(\Delta f \cdot P)/(h\nu B/2\pi e)J$ and the abscissa is the injected carrier density $\Delta n = (J/ewB)^{1/2}$.

IV. Carrier Confinement

In the previous sections we have assumed that the bandgap of the $Al_xGa_{1-x}As$ confining layers is sufficiently large so that the injected carriers are well confined in the active region. However, when either the active layer is very thin or the junction temperature rises, the injected carriers may gain enough energy to leak through the heterostructure barriers. In this section we consider the height of the heterostructure barriers necessary to confine injected carriers in the active region of various widths and at different temperatures.

Previous estimates of the excess current of laser diode at lasing threshold were attempted by two methods: 1) assuming that the electrons and holes escape the heteroboundaries at thermal velocity [22], and 2) assuming that the conduction of the escaping carriers are governed by diffusion processes [23]. The first method yielded an estimated upper limit of the excess current which was an order of magnitude too large compared to experiments while the second method ignored the drift current which, for electrons, is comparable to the diffusion current in our diodes. Since the excitation of carriers into the X conduction band valley is negligible [22], [23], we consider electrons in the Γ conduction band valley and holes in the Γ valance band only. For a symmetrical DH junction under forward bias the quasi-Fermi level of the excess electrons in the p-passive layer (Fig. 1), denoted by δ_P, and that of the excess holes in the n-passive layer, denoted by δ_N, can be written as [22]

$$\begin{aligned} \delta_P &= -E_c + E_a + \phi_P + \phi_n - \phi_p \\ \delta_N &= E_c - E_a + \phi_N - \phi_n + \phi_p. \end{aligned} \tag{21}$$

E_c and E_a are bandgap energies of the confining layers and the active layer, respectively $(E_c > E_a)$. Both E_c and E_a depend on the aluminum arsenide mole fraction x in the form

$$E(x) = 1.424 + 1.266x + 0.26x^2 \text{ eV}. \tag{22}$$

In (21), ϕ_P corresponds to the Fermi level of holes in the p-passive layer with doping concentration P and ϕ_N the Fermi level of electrons in the n-passive layer with doping concentration N. ϕ_n and ϕ_p are quasi-Fermi levels of electrons Δn and holes Δp, respectively, in the active region. The sign conventions are positive for electron Fermi levels above the conduction bandedge and positive for hole Fermi levels above the valance bandedge. The excess electron concentration N' and hole concentration P' in the passive layers are calculated from δ_P and δ_N numerically by the Fermi-Dirac probability distribution, once the values of Δn, Δp, N, P, E_c, and E_a are specified. Since the carrier densities are mostly nondegenerate, parabolic band approximations yield reasonably good results. Degeneracy is considered only for electrons in the active region.

If the injected electron density exceeds the acceptor concentration in the active layer, equal amount of holes must be injected from the other heterojunction (a case of double injection) in order to maintain charge neutrality conditions. In this case the amount of injected electrons Δn is

$$\Delta n = \left(\frac{J}{ewB} \right)^{1/2}. \tag{23}$$

In a practical diode of 50-μm diameter emitting area, the estimated electron density Δn at the safe operating current of 100 mA is approximately 1.7×10^{18} cm^{-3} and 4.5×10^{18} cm^{-3} for $w = 2$ and 0.3 μm, respectively, assuming $B = 5 \times 10^{-11}$ cm^3/s as determined in our experiments (details see Section V). At full power saturation due to thermal heating at 300 mA, Δn would be 2.8×10^{18} cm^{-3} and 8×10^{18} cm^{-3}, respectively.

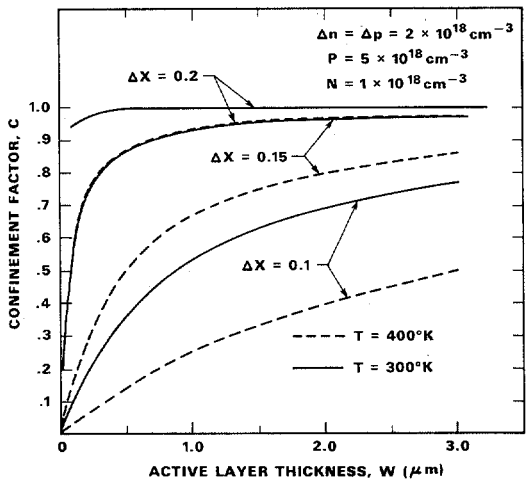

Fig. 6. Confinement factor at 300 and 400 K as a function of the active layer thickness w. Δx is the differential aluminum mole fraction.

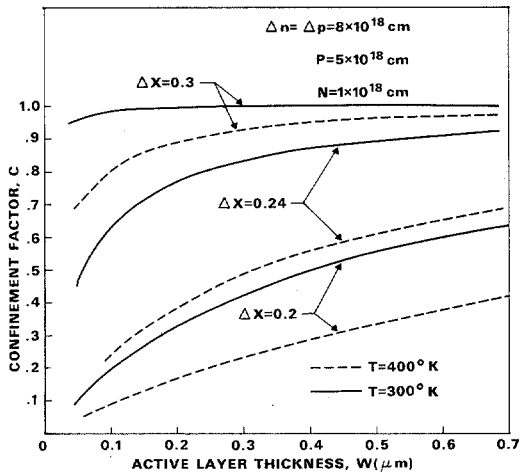

Fig. 7. Confinement factor as a function of the active layer thickness w for $w < 1$ μm. Δx is the differential aluminum mole fraction.

Without the knowledge of the detailed transport mechanism of carriers across the heterostructure barriers, we assume that the excess electron current density to be the sum of the drift current and the diffusion current in the confining layers given by

$$J_n' = qu_n E N' + qD_n \frac{dN'}{dx} \tag{24}$$

where the electron mobility $\mu_n = 3500$ cm^2/V · s has been assumed, and $D_n = \mu_n(kT/e)$. The electric field $E = \rho_P J$ where J is the current density passing through the junction and ρ_P is the resistivity of the p-passive layer. The calculation of excess hole current J_p' is the same as above but replacing N with P, assuming $\mu_p = 250$ cm^2/V · s, and $E = \rho_N J$. The total excess current density necessary to keep constant injected carrier densities Δn and Δp in the active layer is therefore $J' = J_n' + J_p'$. We introduce a "confinement factor" defined in (25)

$$C = \frac{1}{1 + (J'/J)} \tag{25}$$

where J is given by (23). Figs. 6 and 7 give two plots of the "confinement factor" as a function of the active layer thickness w, for $\Delta n = 2 \times 10^{18}$ cm^{-3} and $\Delta n = 8 \times 10^{18}$ cm^{-3}, respectively, Δx is the differential aluminum arsenide mole fraction between the confining and the active layers. These calculations are made for two temperatures, 300 and 400 K. The later temperature is chosen because experiments indicate that for most of our diodes the junction temperature is about 80 to 100 K above ambient when the diode is driven to full power saturation. The other parameters are $P = 5 \times 10^{18}$ cm^{-3} and $N = 1 \times 10^{18}$ cm^{-3}. The heavy doping in the passive layers not only reduces the series resistance, but also enhances carrier confinement [22]. These figures suggest 1) that for $w > 1$-μm good confinement ($C \geqslant 0.8$) over the temperature range of 300 to 400 K can be achieved if $\Delta x \geqslant 0.2$, and 2) that for $0.1 < w < 0.5$-μm good confinement requires $\Delta x \geqslant 0.3$.

V. Experiments

A. Wafer Growth and Diode Fabrication

The DH wafers were grown by liquid phase epitaxy (LPE) using a horizontal sliding boat technique reported elsewhere [24]. All active layers were grown at 800°C with a 0.4°C/min cooling rate. The n-type ⟨100⟩ GaAs substrates were silicon doped at about 2×10^{18} cm^{-3} concentration. The first grown layer was n-type $Al_{0.33}Ga_{0.67}As$, 10–15 μm thick, Te doped at a concentration of $\sim 10^{18}$ cm^{-3}. Next, a p-type $Al_xGa_{1-x}As$ layer was grown ($0 < x < 0.14$) at various thicknesses between 0.3 and 2.5 μm. This "active" layer was prepared with Ge-doping densities ranging from 1×10^{17} cm^{-3} to 2×10^{19} cm^{-3}. The growth of the "active" layer was followed by a $\sim$1.0-μm thick p-type $Al_{0.33}Ga_{0.67}As$ layer doped with Ge to a concentration of about 5×10^{18} cm^{-3}. In some cases a fourth layer, p-type GaAs heavily doped with Ge, was grown for contacting purposes. However, we have found that the fourth layer may not be necessary and ohmic contact directly to the $Al_xGa_{1-x}As$ layer can be made satisfactorily.

All the diodes investigated had the Burrus-type structure, as shown in Fig. 1(a), with a small circular emitting area 50 μm in diameter. This small emitting area was defined by contacting the p^+ surface in the 50-μm diameter window area opened in the silicon oxide layer. Thus the current was restricted to flow in the contacted area only. A "well" was etched in the GaAs substrate up to the n-$Al_{0.33}Ga_{0.67}As$ layer which is transparent to the emitted light.

B. Measurements

The total optical power was measured by a large area, calibrated photodiode placed as close as possible to the emitting "well" of the LED. Maximum power output for all LED's were obtained at 300-mA dc (corresponding to a current density of 15 kA/cm^2) near the point at which power saturation by thermal heating sets in.

For the measurement of the modulation bandwidth the LED was forward biased and modulated by an RF current of 12.4-mA peak-to-peak. Variations of the carrier lifetime as a function of the injection current were evaluated by measuring the bandwidth at various bias currents. The light output was detected by a small area, fast p-i-n photodiode and displayed in frequency domain by means of an RF spectrum analyzer. If the recombination current dominates the LED current, the

TABLE I
SUMMARY OF POWER OUTPUT VERSUS THICKNESS, DOPING CONCENTRATIONS, AND DIFFERENTIAL ALUMINUM MOLE FRACTION

BATCH NO.	ACTIVE LAYER HOLE CONCENTRATION (N_A, cm-3)	DIFFERENTIAL Al MOLE FRACTION Δx	ACTIVE LAYER THICKNESS (μm)	EMISSION WAVELENGTH, λ (μm)	POWER OUTPUT (mW) 50mA	100mA	150mA	300mA
DM-116	$2x10^{17}$	0.2	1.0	.7920	1.8	3.4	4.9	7.6
DM-176	$2x10^{17}$	0.2	1.0	.8080	2.2	4	5.3	7
DM-154	$2x10^{17}$	0.2	1.2	.7874	2.4	4.5	6.2	10.3
DM-148	$2x10^{17}$	0.2	1.6	.7910	2	4.1	5.7	8.8
DM-173	$2x10^{17}$	0.2	2.0	.8230	2.5	5	6.7	12
DM-177	$2x10^{17}$	0.2	2.5	.8120	3.5	6.1	8.6	15
SM-326	$2x10^{17}$	0.3	0.5	.8605	1.8	3.4	6.6	11
SM-331	$2x10^{17}$	0.3	0.3	.8600	2	3.8	5.6	9
SM-332	$2x10^{17}$	0.3	0.3	.8500	2.5	4.5	6.2	-
SM-327	$2x10^{17}$	0.3	0.3	.8500	2.6	4.7	6.6	9.2
SM-340	$2x10^{17}$	0.5	1.6	.8600	2.6	4.6	6.1	8
DM-167	$5x10^{17}$	0.2	1.0	.7970	1.3	2.6	3.2	5.4
DM-156	$5x10^{18}$	0.2	2.0	.7965	1.2	2.2	2.9	4.1
DM-179	$1x10^{19}$	0.2	1.0	.8160	0.5	1.0	1.5	2.5
DM-180	$1.5x10^{19}$	0.2	2.0	.8300	0.4	0.86	1.4	2.8
DM-185	$1.5x10^{19}$	0.3	1.5	.8730	0.8	1.5	2.2	3.8
DM-203	$2x10^{19}$	0.3	1.5	.8970	0.4	0.85	1.2	2.0

RF power at the photodiode output should vary with the RF modulation frequency following the expression

$$P_{\text{elec}}(\omega) = KI_0^2 m^2/(1 + \omega^2\tau^2) \tag{26}$$

where I_0 is the dc bias current, m the modulation index, τ the carrier lifetime, K a proportionality constant, and $\omega = 2\pi f$. The modulation bandwidth Δf is defined as the frequency at which the RF *electrical power* is down by 3 dB, thus $\tau = 1/2\pi\Delta f$.

C. Results

Power Output Versus Active Layer Thickness, Doping Concentrations and the Differential Aluminum Mole Fraction: Table I summarizes the results of typical runs with various active layer thicknesses, doping concentrations, and the differential aluminum mole fraction Δx. The carrier concentrations shown in the second column were inferred from the Hall mobility measured in thin layers which were grown on Cr-doped semi-insulating GaAs substrate at exactly the same growth conditions and with the same amount of Ge in the melt as for the growth of the active layer in the diode sample. The relation between the amount of Ge in the melt and the resulting hole concentration is in good agreement with the published results [25], [26]. The third column gives the difference in the aluminum mole fraction between the confining layers and the active layer. The aluminum mole fraction x is 0.33 in the confining layers for all samples, except sample SM-340 for which $x = 0.5$. The value of x in the active layer ranges between ~0.03 and 0.14 judging by the emission wavelength as listed in the fifth column. At $N_A > 10^{19}$ cm^{-3}, the emission wavelength shifted appreciably toward longer wavelength as seen in Sample DM-179. When the active layer contains 10 percent Al, the highest hole concentration obtained using Ge as dopant was about 1.5×10^{19} cm^{-3}, whereas in pure GaAs, the highest concentration obtained was about 2×10^{19} cm^{-3}.

For each concentration, a number of wafers was grown with various active layer thickness, as shown in the fourth column of Table I. Most of the effort was devoted to optimizing the layer thickness for wafers with lightly doped active regions. These LED's, emitting near 8050-Å wavelength, were used for pump diode of an end-pumped Nd:YAG fiber laser [27]. Care was taken in the "well" etching so that the light output was optimized by step etching. Nevertheless, it was often found that the output power may vary by as much as 50 percent within a single batch. The last four columns in Table I list the power output, at 50, 100, 150, and 300 mA, respectively, for each batch. At 100-mA drive the output is linear with current indicating that the junction heating is not significant (~10°C rise in junction temperature).

The power output (at 100 mA) versus the active layer thickness with $N_A \sim 2 \times 10^{17}$ cm^{-3} doping is plotted in Fig. 8(a). The numerals are wafer numbers as listed in Table I. The carrier recombination times were obtained both at very low injection current (few milliampere current) and at high injection current (100 mA) by the modulation bandwidth measurement described in Section III. At the low injection levels, the recombination is primarily nonradiative, thus the measured lifetime approximates the nonradiative recombination time which is plotted as a function of the active layer thickness in Fig. 8(b). On the other hand, at the 100-mA high-injection level, the radiative recombination is enhanced, thus the total carrier lifetime is decreased (details in the next section). The internal quantum efficiency taken as $(1 - \tau/\tau_{nr})$ can be calculated from the two lifetime results, and it is also plotted in Fig. 8(b) as a function of the active layer thickness. The nonradiative recombination time shown in Fig. 8(b) varies approximately linearly with w, for $w \geqslant 1$ μm, suggesting that it is primarily due to the interfacial recombination at the heterointerfaces. Using $\tau_{nr} = w/2s$, the result of Fig. 8(b) gives $s = 2 \times 10^3$ cm/s. For thin active layers s is even less than the above value, indicating some improvement of the interfacial quality over that of the thick layers. This result is in agreement with that found in [5]. In order to prevent carrier leakage in the thin active region Δx is increased to 0.3 for all wafers with $w \leqslant 0.5$ μm. (See Section IV.) The interface quality did not seem to degrade with increasing Δx up to a value as high as 0.5. (Wafer SM-340.)

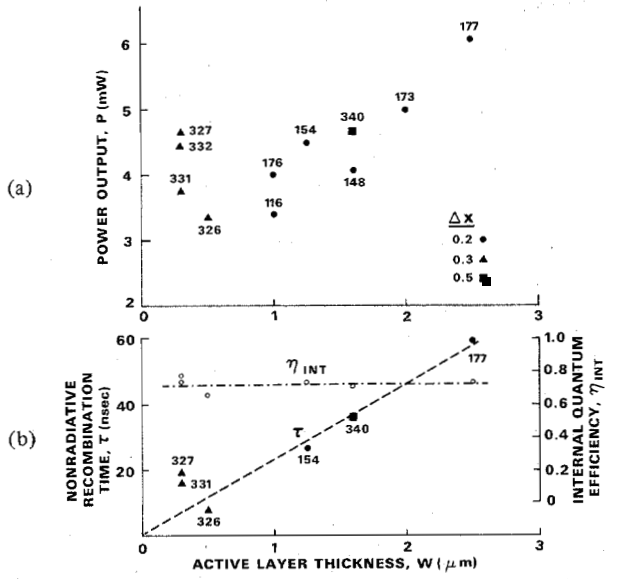

Fig. 8. (a) Power output (at 100 mA) as a function of the active-layer thickness of experimental diodes. The numerals are batch number as listed in Table I. (b) Measured nonradiative recombination time and the calculated internal quantum efficiency as a function of the active-layer thickness.

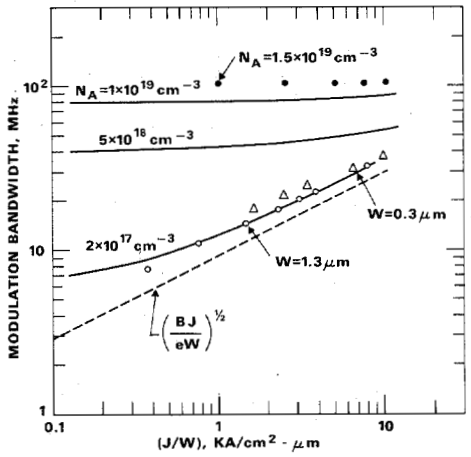

Fig. 9. The modulation bandwidth as a function of the normalized current density (J/w).

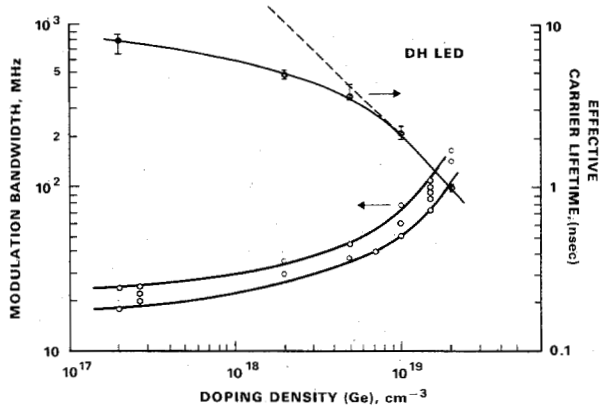

Fig. 10. Modulation bandwidth and carrier lifetime at 100-mA drive current as a function of the doping concentration in the active region.

The internal quantum efficiency, about 70 percent, is independent of the active layer thickness, as a consequence of the small value of the interfacial recombination velocity s. It leads us to believe that the relatively large variation in the output power is probably due to variations in the light extraction efficiency of these diodes because our device fabrication process was not strictly controlled. The external quantum efficiency amounts to 4-5 percent.

Modulation Bandwidth and Carrier Lifetime: The radiative recombination time of the carriers is a function of Ge concentration and the injection level as given by (17). Using the bandwidth definition of (15), the bandwidth is plotted against (J/w) for various doping concentrations in Fig. 9. It can be seen that at 2×10^{17} cm^{-3} doping the bandwidth increases as $(J/w)^{1/2}$, whereas at high doping concentrations, the bandwidth becomes independent of (J/w). Experimentally measured bandwidth on diodes with low and high doping concentrations (shown by open and solid circles) agreed well with calculated results, assuming $s = 2 \times 10^3$ cm/s and $B = 5 \times 10^{-11}$ cm^3/s.

It is obvious, that at low doping concentrations heavy injection increases not only the efficiency but also the modulation speed. However, the maximum current density at which the diodes can be safely operated is likely to be limited by thermal heating. With our present fabrication technique, the operating current density is at about 7.5 kA/cm^2. Thus for a thick (2 μm) active layer, the modulation bandwidth would be about 25 MHz, whereas for a thin (0.3 μm) active layer, the modulation bandwidth would be near 60 MHz.

For modulation bandwidth above 100 MHz, it is necessary either to decrease the active layer down to 0.1 μm or less [12], or to increase the doping concentration. For the latter case, we have found that the bandwidth increased with N_A as shown in Fig. 10. All diodes plotted in Fig. 10 have thick (1.5-2 μm) active region, and the bandwidths Δf, shown in the lower curves are measured at 100-mA bias (5 kA/cm^2). The effective carrier lifetimes are shown by the error bars on the upper curve by converting $\tau_{\text{eff}} = 1/2\pi\Delta f$. The upper solid curve is computed by (16) and (17) using $s = 2 \times 10^3$ cm/s, $B = 5 \times 10^{-11}$ cm^3/s, $J = 5$ kA/cm^2, and $w = 2 \times 10^{-4}$ cm. It is seen that the agreement is quite satisfactory. The recombination probability constant B is concentration dependent [25] and has been found by various investigators to be in the range of 6.4×10^{-11} cm^3/s [28] to 1.3×10^{-10} cm^3/s [29].

Maximum Output Power and Bandwidth: The maximum output power emitted into the air at 300-mA dc drive current versus the 3-dB modulation bandwidth at the same dc bias current is plotted in Fig. 11 for diodes with various doping concentrations and thicknesses. Maximum output power of 15 mW with a modulation bandwidth of 17 MHz was obtained with the lowest doping density of about 2×10^{17} cm^{-3}. As doping density increased, the modulation bandwidth increased at the expense of output power. At 2×10^{19} cm^{-3} doping, the bandwidth reached 170 MHz with a power output of 2 mW. Thermal heating apparently caused the output to saturate near a drive current of 300 mA. (The excessive heating at this high-drive current may damage the junction and shorten the operating life of these devices. A safer operating point is at a current of about 150 mA.) For the lightly doped diodes operating at 150 mA, the bandwidth, depending on the square root of the injection current density, becomes a factor 1.4 smaller than the values shown in Fig. 11.

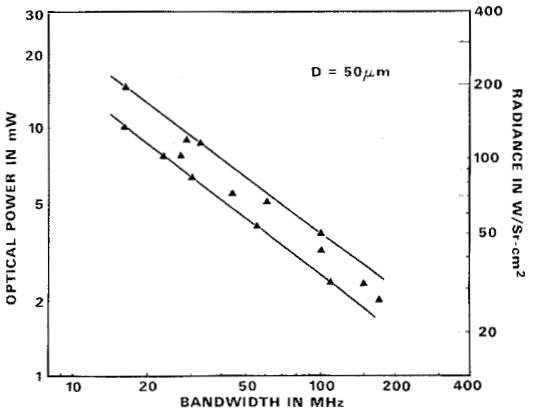

Fig. 11. Optical power emitted into air (left-hand coordinate) and on-axis radiance (right-hand coordinate) of DH Burrus-type LED's at 300-mA dc drive (50-μm diameter emitting area) as a function of 3-dB modulation bandwidth at the same bias current.

At this point, it is appropriate to compare the optimum doping levels of DH and homojunction LED's of the same geometry. In the Zn-diffused homojunction GaAs LED's reported previously [30], it was found that maximum efficiency and power were obtained with Zn diffusion into n-type substrate with doping density about 2×10^{18} cm^{-3} to 4×10^{18} cm^{-3} [31]. This is because on the one hand the nonradiative recombination due to large surface recombination dominates at low doping levels, at which the radiative recombination time is long, and the recombination region extends to several diffusion lengths, resulting in large reabsorption at low doping concentrations. On the other hand, Auger recombination becomes important at doping levels higher than 5×10^{18} cm^{-3}. In a DH LED, however, the surface recombination can be made small and, simultaneously, the internal efficiency is increased by the enhancement of the radiative recombination rate due to increased carrier densities achieved by carrier confinement. Thus the maximum efficiency and power are obtained with the active region doped lightly in the 10^{17} cm^{-3} range. With a thin active layer, the reabsorption is negligible.

For our experimental diodes, the ratio of the power bandwidth product between units with a heavily doped active layer and units with a lightly doped active region is approximately two to one, while the theoretical value of this ratio is four to one (see Fig. 5). This discrepancy may be attributed to the fact that the injection efficiency is lower for the heavily doped diodes and nonradiative recombination may be introduced by heavy doping.

Spectral Width: The half-height-full-width emission spectrum was found to increase from 250 Å at 1×10^{17} cm^{-3} doping concentration to over 500 Å at a doping level of 2×10^{19} cm^{-3}. The high modulation rate capability of the LED's, unfortunately, will be severely limited by the material dispersion of the transmission fiber if the LED is to be used in a light wave communication system at 0.8–0.9-μm wavelength. This obstacle may be overcome by using LED's emitting at longer wavelengths [32], [33].

VI. Discussions and Conclusions

We have considered the device parameters relevant to the efficiency and modulation bandwidth of AlGaAs–GaAs DH LED's. These parameters are self absorption, heterointerface recombination velocity, doping concentration, active layer thickness, injection current density, and carrier confinement. Some of these parameters are interrelated. In contrast to diffused homojunction devices, higher power is obtained with a lightly doped active region in the DH LED's. This is because, first, the good heterointerface quality reduces the nonradiative recombination at surfaces; second, confinement of electrons is possible in a thin active layer, which increases the density of injected carriers; third, as a consequence of the increased carrier density the radiative recombination rate is enhanced and the carrier lifetime shortened. Hence the power bandwidth product is improved. The confinement of injected carriers up to 8×10^{18} cm^{-3} dictates that the differential aluminum arsenide mole fraction $\Delta x \geq 0.2$ for active layer thickness greater than 1 μm, and $\Delta x \geq 0.3$ for active layer thickness thinner than 0.5 μm. The interfacial recombination velocity $s = 2 \times 10^3$ cm/s for $w > 1$ μm and is smaller for $w < 1$ μm [5]. The effect which has not been considered in the analysis is the lateral diffusion of carriers at high carrier densities. The lateral diffusion would reduce the effective current density and thus reduce both efficiency and bandwidth. Saturation of output power is primarily due to thermal heating although other factors such as carrier leakage and lateral diffusion may be important also. Detailed treatment has not been attempted at this time.

Our experimental diodes produced maximum output power of 15 mW into the air with a 17-MHz modulation bandwidth. A higher modulation bandwidth of 170 MHz was obtainable at a reduced output of 2 mW. This was accomplished by increasing the Ge doping to about 2×10^{19} cm^{-3} in the active layer. The increased modulation bandwidth is accompanied by an increase in the light spectral width from 250 to 500 Å.

Acknowledgment

The authors wish to thank C. A. Burrus for many helpful discussions, M. A. Pollack for Hall measurements, D. L. Rode for supplying programs in computing Fermi levels, W. S. Holden and F. Favire for diode fabrication, and H. E. Kehlenbeck for device evaluations.

References

[1] C. A. Burrus and B. I. Miller, "Small-area double-heterostructure Aluminum-Gallium-Arsenide electroluminescent diode sources for optical-fiber transmission lines," *Opt. Commun.*, vol. 4, no. 4, pp. 307–309, Dec. 1971.

[2] W. Harth and J. Heinen, "Investigation on GaAs:GaAlAs single-heterostructure light emitting diode for optical communication systems," *Electron. Commun.*, vol. 29, pp. 989–992, Dec. 1975.

[3] W. Harth, W. Huber, and J. Heinen, "Frequency response of GaAlAs light-emitting diodes," *IEEE Trans. Electron Devices* (Corres.), vol. ED-23, pp. 478–480, Apr. 1976.

[4] F. D. King, A. J. SpringThorpe, and O. I. Szentesi, "High-power long-lived double-heterostructure LED's for optical communications," *Tech. Dig.*, Int. Electron Device Meet., 1975, pp. 480–481, Dec. 1975.

[5] M. Ettenberg and H. Kressel, "Interfacial recombination at AlGaAs/GaAs heterojunction structures," *J. Appl. Phys.*, vol. 47, pp. 1538–1544, Apr. 1976.

[6] M. Ettenberg, H. Kressel, and S. L. Gilbert, "Minority carrier diffusion length and recombination lifetime in GaAs:Ge prepared by liquid-phase epitaxy," *J. Appl. Phys.*, vol. 44, pp. 827–831, Feb. 1973.

[7] H. C. Cassey, Jr., B. I. Miller, and E. Pinkas, "Variation of minority-carrier diffusion length with carrier concentration in GaAs liquid-phase epitaxial layers," *J. Appl. Phys.*, vol. 44, pp. 1281–1287, Mar. 1973.
[8] J. Zucker, R. B. Lauer, and J. Schlafer, "Response time of Ge-doped (Al, Ga) As-GaAs double-heterostructure LED's," *J. Appl. Phys.*, vol. 47, pp. 2082–2084, May 1976.
[9] T. P. Lee, "Effect of junction capacitance on the rise time of LED's and on the turn-on delay of injection lasers," *Bell Syst. Tech. J.*, vol. 54, pp. 53–68, Jan. 1975.
[10] C. A. Burrus, T. P. Lee, and W. S. Holden, "Direct-modulation efficiency of LED's for optical fiber transmission applications," *Proc. IEEE* (Lett.), vol. 63, pp. 329–331, Feb. 1975.
[11] R. C. Goodfellow and A. W. Mabbitt, "Wide-band-width high radiance gallium-arsenide light emitting diodes for fiber-optic communication," *Electron. Lett.*, vol. 12, pp. 50–51, Jan. 1976.
[12] H. F. Lockwood, J. P. Wittke, and M. Ettenberg, "LED for high data rate optical communications," *Opt. Commun.*, vol. 16, pp. 193–196, Jan. 1976.
[13] A. A. Bergh and P. J. Dean, "Light-emitting diodes," *Proc. IEEE*, vol. 60, pp. 156–223, Feb. 1972.
[14] H. C. Casey, Jr., and F. A. Trumbore, "Single crystal electroluminescent materials," *Mater. Eng.*, vol. 6, pp. 69–109, 1970.
[15] H. C. Casey, Jr., D. D. Sell, and K. W. Wecht, "Concentration dependence of the absorption coefficient for n and p-type GaAs between 1.3 and 1.6 eV," *J. Appl. Phys.*, vol. 46, pp. 250–257, Jan. 1975.
[16] A. Many, Y. Goldstein, and N. B. Grover, *Semiconductor Surfaces*. New York: North-Holland, 1965, p. 260.
[17] W. Harth, J. Heinen, and W. Huber, "Influence of active-layer width on the performance of homojunction and single-heterojunction GaAs light emitting diodes," *Electron. Lett.*, vol. 11, pp. 23–24, Jan. 1975.
[18] H. Namizaki, M. Nagano, and S. Nakahara, "Frequency response of $Ga_{1-x}Al_xAs$ light-emitting diodes," *IEEE Trans. Electron Devices*, vol. 21, pp. 688–691, Nov. 1974.
[19] Y. S. Liu and D. A. Smith, "The frequency response of an amplitude-modulated GaAs luminescence diode," *Proc. IEEE* (Lett.), vol. 63, pp. 542–544, Mar. 1975.
[20] R. N. Hall, "Recombination processes in semiconductors," *Proc. IEE*, vol. 106 (Supplement), pp. 923–931, Mar. 1960.
[21] H. Namizaki, H. Kau, M. Ishii, and A. Ito, "Current dependence of spontaneous lifetimes in GaAs-AlGaAs double heterostructure lasers," *Appl. Phys. Lett.*, vol. 24, pp. 486–487, May 1974.
[22] D. L. Rode, "How much Al in the AlGaAs-GaAs laser?" *J. Appl. Phys.*, vol. 45, pp. 3887–3891, Sept. 1974.
[23] A. R. Goodwin, J. R. Peters, M. Pion, G. H. B. Thompson, and J. E. A. Whiteaway, "Threshold temperature characteristics of double heterostructure $Ga_{1-x}Al_xAs$ lasers," *J. Appl. Phys.*, vol. 46, pp. 3126–3131, July 1975.
[24] B. I. Miller, E. Pinkus, I. Hayashi, and R. J. Capik, "Reproducible liquid phase epitaxial growth of double heterostructure GaAs-$Al_xGa_{1-x}As$ laser diode," *J. Appl. Phys.*, vol. 43, pp. 2817–2826, June 1972.
[25] C. J. Hwang and J. C. Dyment, "Dependence of threshold and electron lifetime on acceptor concentration in GaAs-$Ga_{1-x}Al_xAs$ lasers," *J. Appl. Phys.*, vol. 44, pp. 3240–3244, July 1973.
[26] D. R. Ketchow, "Germanium-doped GaAs for p-type ohmic contacts," *J. Electrochem. Soc. Solid-State Sci. Tech.*, vol. 121, pp. 1237–1239, Sept. 1974.
[27] J. Stone, C. A. Burrus, A. G. Dentai, and B. I. Miller, "Nd:YAG single-crystal fiber laser," *Appl. Phys. Lett.*, vol. 29, pp. 37–39, July 1976.
[28] H. C. Casey, Jr. and F. Stern, "Concentration dependent absorption and spontaneous emission of heavily doped GaAs," *J. Appl. Phys.*, vol. 47, pp. 631–643, Feb. 1976.
[29] G. A. Acket, W. Nijam, and H. 't Lam, "Electron lifetime and diffusion constant in Ge-doped GaAs," *J. Appl. Phys.*, vol. 45, pp. 3033–3040, July 1974.
[30] C. A. Burrus, "Radiance of small area high-current-density electroluminescent diodes," *Proc. IEEE* (Lett.), vol. 60, pp. 231–232, Feb. 1972.
[31] C. A. Burrus, private communication.
[32] D. N. Payne and W. A. Gambling, "Zero material dispersion in optical fibers," *Electron. Lett.*, vol. 11, pp. 176–178, Apr. 1975.
[33] W. M. Muska, T. Li, T. P. Lee, and A. G. Dentai, "Material-dispersion-limited operation of high-bit-rate optical-fiber data links using LEDs," *Electron. Lett.*, vol. 13, pp. 605–607, Sept. 1977.

Characteristics of Integrated MOM Junctions at dc and at Optical Frequencies

MORDEHAI HEIBLUM, SHIHYUAN WANG, MEMBER, IEEE, JOHN R. WHINNERY, FELLOW, IEEE, AND T. KENNETH GUSTAFSON

Abstract—**We present a new metal-oxide-metal device (Ni-NiO-Ni, "Edge MOM") which is stable, reproducibly fabricated, and with a 10^{-10}-cm^2 tunneling area. Performing detection experiments, the device's nonlinear I-V characteristic is shown to be invariant at audio frequencies, 10.6, 3.39, and 0.6328 μm. Similar devices with 10^{-8}-cm^2 tunneling areas perform as well as the Edge MOM's in the visible and the near-infrared range, but deteriorate in performance at the 10-μm range. A dominant competing effect is a thermal-induced signal, which increases with frequency and temperature. Coupling mechanisms at the various regimes are investigated.**

The device can serve as a broad-band detector and mixer, and might in the future be a basic element of broad-band amplifiers and oscillators.

Manuscript received July 18, 1977; revised November 4, 1977. This work was supported in part by the Air Force Office of Scientific Research under Grant F44620-76-C-0100, National Aeronautics and Space Administration Grant NSG-2151, and National Science Foundation Grant ENG72-03960-A01.

The authors are with the Department of Electrical Engineering and Computer Sciences, and the Electronics Research Laboratory, University of California, Berkeley, CA 94720.

I. Introduction

We report new work on the metal-oxide-metal (MOM) device. This is one of the most interesting of recent devices, and one for which there is still much discussion about the mechanism of operation.

0018-9197/78/0300-0159$00.75 © 1978 IEEE